Nuclear Instruments and Methods in Physics Research A 609 (2009) 244–249

Contents lists available at ScienceDirect

Nuclear Instruments and Methods in Physics Research A

journal homepage: www.elsevier.com/locate/nima

Statistical analysis of the Doppler broadening coincidence spectrum of electron–positron annihilation radiation in silicon

E. do Nascimento [a,b,*], O. Helene [a], V.R. Vanin [a], M.T.F. da Cruz [a,1], M. Moralles [c]

[a] Instituto de Física, Universidade de São Paulo, CP 66318, CEP 05315-970, São Paulo, SP, Brazil
[b] Facultad de Física, Universitat de Barcelona, CEP 08028, Barcelona, Spain
[c] Instituto de Pesquisas Energéticas e Nucleares-IPEN/CNEN-SP, CEP 05508-000, São Paulo, SP, Brazil

ARTICLE INFO

Article history:
Received 27 March 2008
Received in revised form
21 July 2009
Accepted 28 July 2009
Available online 4 August 2009

Keywords:
Doppler broadening
Positron annihilation
Least-squares method
Silicon

ABSTRACT

We report a statistical analysis of Doppler broadening coincidence data of electron–positron annihilation radiation in silicon using a ^{22}Na source. The Doppler broadening coincidence spectrum was fit using a model function that included positron annihilation at rest with 1s, 2s, 2p, and valence band electrons. In-flight positron annihilation was also fit. The response functions of the detectors accounted for backscattering, combinations of Compton effects, pileup, ballistic deficit, and pulse-shaping problems. The procedure allows the quantitative determination of positron annihilation with core and valence electron intensities as well as their standard deviations directly from the experimental spectrum. The results obtained for the core and valence band electron annihilation intensities were 2.56(9)% and 97.44(9)%, respectively. These intensities are consistent with published experimental data treated by conventional analysis methods. This new procedure has the advantage of allowing one to distinguish additional effects from those associated with the detection system response function.

1. Introduction

Positron annihilation spectroscopy is a well-established technique that has been extensively used to probe condensed matter systems [1,2]. With the introduction of a second Ge detector enabling the measurement of both annihilation photons [3], Doppler broadening spectroscopy takes advantage of coincidence techniques, adding characteristics of high selectivity of the detected signal and great improvement of the analysis procedure. A gain of $\sim\sqrt{2}$ in the combined energy resolution for the observation of the annihilation peak and an important reduction in the background are obtained when compared with measurements taken with only one Ge detector. Another important feature that has not received much attention is that in these coincidence measurements one obtains two-dimensional (2D) energy spectra. Hence, the Doppler broadening coincidence spectrum (DBCS) shows effects of the electron–positron annihilation process and the detection system, which can be broken down into their components because they are distributed throughout the 2D spectrum. In the annihilation processes, both energy and momentum are conserved [1]; however, precise measurements in solids [4–6] have demonstrated that electron–positron annihilation radiation has an energy deficit, with the total photon energy below $2m_0c^2$. This deficit is due to the binding energies of the annihilated electrons [6,7] and this information is always present in the photons of annihilations that occur in surface and bulk metals or semiconductors, as well as information related to the momentum of electron–positron pairs. However, these properties have never been used for the analysis of the Doppler broadening spectrum.

The behavior of positrons near nuclei is essentially independent of the atomic environment and, therefore, the overlaps of their wavefunctions with the various core states of an atom in a solid are well represented in a purely atomic description [8]. On the other hand, information about the atomic environment can be obtained from the contribution of the valence/conduction band to Doppler broadening in the annihilation photon spectrum. Thus, in this work, we have applied a statistical treatment similar to that used for the analysis of the DBCS measured in aluminum [9–11], where a model function was fit to the experimental spectrum using a non-linear least-squares method to get information about the intensities of positron annihilation with 1s, 2s, 2p, and valence band electrons in silicon. The fitting procedure is similar to the method widely used in positron lifetime spectroscopy, for which several computer programs based on non-linear fitting routines are available [1].

In this work, we performed measurements on a Czochralski-grown silicon crystal (Cz-Si) sample. Silicon is a semiconductor of great technological importance [12–19] and has an electronic

* Corresponding author at: Instituto de Física, Universidade de São Paulo, CP 66318, CEP 05315-970, São Paulo, SP, Brazil.
E-mail address: eduardon@if.usp.br (E. do. Nascimento).
[1] Deceased.

0168-9002/$ - see front matter © 2009 Elsevier B.V. All rights reserved.
doi:10.1016/j.nima.2009.07.051

configuration that differs from that of aluminum by one excess electron, requiring modifications in the description of core electrons. This choice was due to the fact that, at the beginning of semiconductor studies with positrons, the use of models developed for metals and applied to semiconductors led to false results and mistaken interpretations about semiconductors [1]. As in the case of aluminum, our goal in this work is to accomplish a realistic description of the DBCS of electron–positron annihilation photons in silicon that, together with information on the response function of the detection system, allows one to directly obtain the annihilation rates with all electrons and their momentum distributions from this spectrum.

2. Method

2.1. General

In positron annihilation experiments, the vast majority of positrons penetrate the sample, thermalize very quickly (within a few ps) [1], and diffuse before annihilation. In DBCS, both annihilation photons are measured in coincidence using two Ge detectors positioned collinearly with the sample.

Let E_1 and E_2 be the energies of the annihilation photons observed by detectors 1 and 2, respectively. For thermalized positrons, the energies of the emitted photons of the electron–positron annihilation are given by

$$E_{1,2} = m_0c^2 - \frac{B_i}{2} \pm \frac{p_z c}{2} \quad (1)$$

where m_0c^2 is the electron rest mass energy, B_i the electron binding energy, c the speed of light, and p_z the momentum component of the positron–electron pair in the direction of the emitted annihilation photons. It is useful to define two other energies: the sum, $E_1+E_2 = 2m_0c^2-B_i$, and the difference, $E_1-E_2 = p_zc$. The sum energy is equal to the total energy of the electron–positron system before annihilation. The Doppler broadening profile is determined with the help of the energy difference, where the energy of one annihilation photon is Doppler shifted upwards by $+p_zc/2$, and that of the other photon is Doppler shifted downwards by $-p_zc/2$. The energies of both annihilation photons and the time interval between their detections are recorded, and the event is stored in a 2D array [9–11].

Fig. 1 shows the contour plot of the experimental DBCS obtained from a measurement performed with a positron source

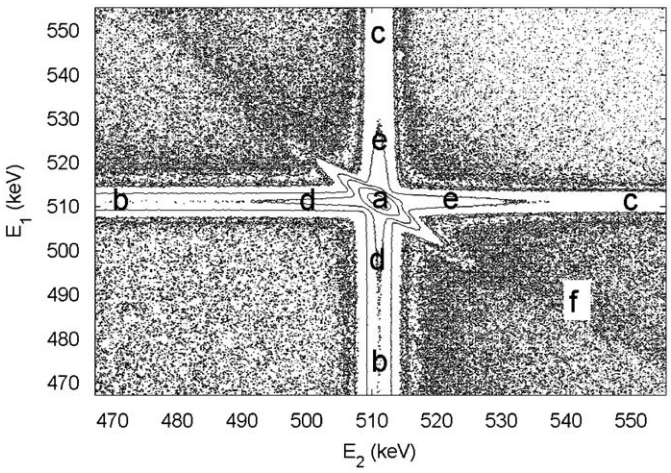

Fig. 1. Contour plot of the experimental DBCS of annihilation radiation in silicon (Cz-Si). E_1 denotes the energy measured by detector 1 and E_2 that by detector 2.

deposited between two silicon disks. In this figure, the DBCS may be interpreted as follows: the peak identified as a has a broadening along the line $E_1+E_2 = 2m_0c^2$ due to Doppler shift of the annihilation radiation. Furthermore, at both ends of this line there are subtle structures corresponding to backscattered annihilation photons. The two ridges extending from the peak towards lower energies ($E_1 < m_0c^2$ or $E_2 < m_0c^2$), identified as b, are called internal ridges, mainly due to coincidence events where one of the annihilation photons suffers Compton scattering. Since we have used ^{22}Na as the positron source, which emits a 1274 keV gamma-ray in its decay, ridges are formed towards higher energies. These are the external ridges (c in Fig. 1), which are due to the coincidence of one annihilation photon with a Compton-scattered 1274 keV gamma-ray. The spectrum also contains exponential tails due to a ballistic deficit, pulse-shaping problems (d in Fig. 1), and pileup (e in Fig. 1).

Although most positrons thermalize before annihilation, there is a small fraction that annihilate before thermalizing. This is the so-called in-flight positron annihilation. When positrons annihilate in flight with a low-momentum electron two photons with energies E_1 and E_2 are emitted and the total energy is given by

$$E_1 + E_2 = 2m_0c^2 + K_+ - B_i \quad (2)$$

where K_+ is the positron kinetic energy at the instant of annihilation. With a small number of events and a larger energy spread [20–24], in-flight positron annihilation is usually masked by the background arising from thermalized positron annihilation. These annihilations are distributed along a circular arc near the 511–511 keV peak in the DBCS (f in Fig. 1).

Fig. 1 also shows a background between the internal ridges that is mainly associated with Compton scattering of both photons in coincidence. There is even more information in this spectrum, although too subtle to be visually noticed, as the various distributions related to annihilation with core electrons are shifted off the line $E_1+E_2 = 2m_0c^2$ by their binding energies as discussed below.

2.2. Experimental setup

A 10 μCi (3.7×10^5 Bq) ^{22}NaCl source was placed between two silicon (Cz-Si) disks, both 2 mm thick. The crystals were positioned with their orientation (111) collinear with the axes of the detectors. Positron lifetime measurements were performed by means of the 1274 keV–511 keV coincidence using a spectrometer with one plastic scintillator and one BaF_2 detector. This system had a time resolution of 360 ps. Three lifetime components plus background were fit to a spectrum with 1.1×10^7 counts. The lifetime components were exponential functions convoluted with a Gaussian function that approximately describes the response function of the time measurements obtained with the spectrometer. The reduced χ^2 obtained in the fit performed in the time range −150 ps to 18 ns was 1.07 with 1357 degrees of freedom. The results indicate that 98.38(20)% of the positrons decay with the characteristic lifetime of annihilation in the silicon bulk. The other components have lifetimes of 552(20) ps and 3.06(19) ns with intensities of 1.36(16)% and 0.26(4)%, respectively, corresponding to minor annihilation contributions in NaCl surfaces and defects. These results confirmed the good quality of the silicon crystal and indicated successful NaCl deposition onto the sample.

The coincident Doppler broadening measurement was performed using a detection system that consisted of two HPGe Ortec detectors (detector 1 with 50 cm^3 and detector 2 with 164 cm^3), analog-to-digital converters (ADC-Ortec AD413), a spectroscopy amplifier (Ortec 673), a fast-filter amplifier (FFA-Ortec 579), a

constant fraction discriminator (CFD-Ortec 584), a custom-built CAMAC-to-PC controller (Multi), and a computer system. The amplifiers and the ADCs were used to measure the energies of the photons, and the FFAs and the CFDs, together with the Multi module, were employed to determine the coincidence time. The counting rate during acquisition of the spectrum was about 1.5×10^3 counts/s. The detectors were placed 10 cm apart, with the sample placed halfway between them. When a coincidence was detected, the energies E_1 and E_2 and the timing information were recorded. An ^{192}Ir source was measured together with a ^{22}Na source at the same time during the experiment to provide energy and width detector calibration references. The energy resolution (FWHM) of detector 1 was 1.38(1) keV for the annihilation peak and that of detector 2 was 1.45(1) keV at 511 keV.

After amplification and digitization, the data were fed into the Multi controller, which contains the coincidence electronics. The time resolution of the system was ~18 ns. The true-event coincidence window was set between −75 and +75 ns and the accidental-event windows were set between +85 and +160, and −85 and −160 ns. The accidental events were subtracted from the DBCS fit in this study. The pileup rejection signals of the spectroscopy amplifiers were used to gate the ADC and their baseline restorer (BLR) circuits were used. The shaping time of the spectroscopy amplifiers was 2 μs.

The measurements in coincidence lasted for about 220 h, divided into 3.6 min runs, and more than 8.1×10^7 counts in the annihilation peak were acquired. The first step in the offline analysis was to check the system stability during acquisition by fitting the annihilation peak in each 3.6 min run; any spectrum whose FWHM varied significantly was discarded and when the peak position changed significantly from its average all energy bins were relocated to account for small displacements in the peaks. Even with very large χ^2, the position parameters and FWHMs are very sensitive to alterations in the spectra.

2.3. Model

The DBCS was modeled by a 2D function that, after convolution with the response function of the detector system, was fit to the experimental spectrum. The model function included at-rest positron annihilation with core and valence band electrons and in-flight positron annihilation.

The probability density function of positron annihilation with valence band electrons was fit by

$$f_v(E_1,E_2)=\frac{A_v e^{-(E_1-E_2)^2/2\sigma_v^2}}{\sqrt{2\pi}\sigma_v}+\sum_{i=1}^{3}C_i(E_1-E_2-\alpha_i)(E_1-E_2+\alpha_i) \quad (3)$$

along the line E_1+E_2+$B_g=1022$ keV, where B_g is the gap energy of silicon [25] and α_i are the cutoff parameters ($C_i=0$ when $|E_1-E_2|>\alpha_i$). Positron annihilation with core electrons was fit by

$$f_{nl}(E_1,E_2)=\frac{A_{nl}e^{-(E_1-E_2)^2/2\sigma_{nl}^2}}{\sqrt{2\pi}\sigma_{nl}} \quad (4)$$

along the line E_1+E_2+$B_{nl}=1022$ keV, where B_{nl} is the nl-orbital binding energy [26] and nl stands for 1s, 2s, and 2p. Finally, events due to in-flight positron annihilation are located within a circle centered at $(3m_0c^2/2,\ 3m_0c^2/2)$ with radius $m_0c^2/\sqrt{2}$ [11]. These events were fit by

$$f_f(E_1,E_2)=A_f e^{-\lambda d} \quad (5)$$

where

$$d=\frac{m_0c^2}{\sqrt{2}}-\sqrt{\left(E_1-\frac{3m_0c^2}{2}\right)^2+\left(E_2-\frac{3m_0c^2}{2}\right)^2} \quad (6)$$

Therefore, the adjustable parameters are A_v, σ_v, C_i, α_i, A_{nl}, σ_{nl}, A_f, and λ.

2.4. Response function

The response functions for each detector were represented by the sum of Gaussian and non-Gaussian terms [9–11]. The Gaussian term has two parameters that correspond to detector resolution. The non-Gaussian term is due to ballistic deficit, scattering, pileup, and incomplete charge collection, which was fit using two internal ($E_{1,2}<m_0c^2$) and two external ($E_{1,2}>m_0c^2$) exponential tails for each detector, totaling 16 parameters. Two internal and two external ridges along the lines $E_1=511$ keV and $E_2=511$ keV, with amplitudes proportional to the peak intensity, were included in the fit to take into account events where an annihilation photon was detected in coincidence with another annihilation photon or a 1274 keV gamma-ray that was Compton scattered, resulting in four intensity parameters. We assumed that the background is proportional to the ridges, with only one fit parameter to represent it [9–11]. Two parameters, corresponding to the peak position at the two energy axes, were fit. Furthermore, the parameter corresponding to the slope of the E_1+$E_2=2m_0c^2$ line relative to the energy axes was fit due to the small gain difference between both detectors. The backscattering was described by a parabola along the line E_1+$E_2=1022$ keV with its axis parallel to the number of counts axis and crossing the (E_1,E_2) plane at (m_0c^2,m_0c^2). Only one parameter was fit, corresponding to the quadratic term.

The functions $f_{1s,2s,2p,v,f}$, the four ridges, the eight exponential tails, the background, and the backscattering were summed and convoluted with the detector response functions, described by two Gaussians. The parameters of the resulting convoluted function were fit to the experimental data. The fitting parameters were four amplitudes of the annihilation distributions (A), four width parameters of the annihilation distributions (σ), six parabolic parameters (three amplitudes and three cutoff parameters), two in-flight annihilation parameters, two background parameters, one backscattering parameter, two peak positions on the two energy axes, one slope parameter of the E_1+$E_2=1022$ keV line with respect to the energy axes, sixteen exponential tail parameters (eight amplitudes and eight attenuation factors), two detector resolution parameters, and four parameters for the ridge intensities. The fitting procedure follows the least-squares method. The electron binding energies were obtained from the literature [26].

3. Results and discussion

The fitting function is the convolution of the model function plus the background with the detector system response function. This function was fit considering a 90 keV × 90 keV region around the two-photon annihilation peak and using the non-linear parameter estimation method [27]. Fig. 2 shows the contour plot of the DBCS fit. The required partial derivatives were evaluated numerically. Uncertainties and covariances of the parameters were calculated using the procedure described in Ref. [28].

The χ^2 value was calculated using the expression

$$\chi^2=\sum_{i,j}\frac{(n_{ij}-F_{ij})^2}{F_{ij}+2a_{ij}} \quad (7)$$

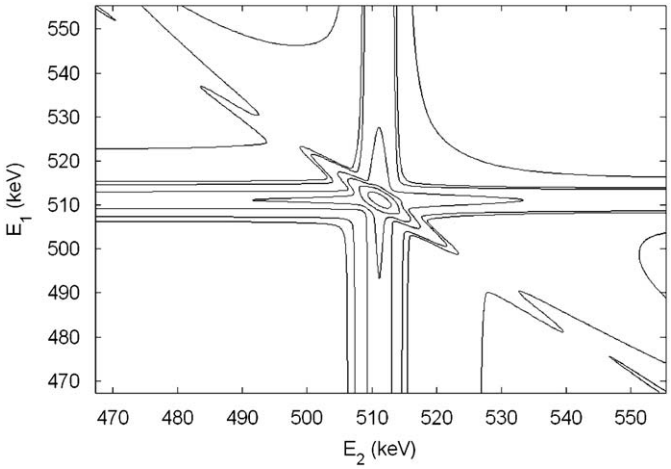

Fig. 2. Fit of the DBCS of annihilation radiation in silicon.

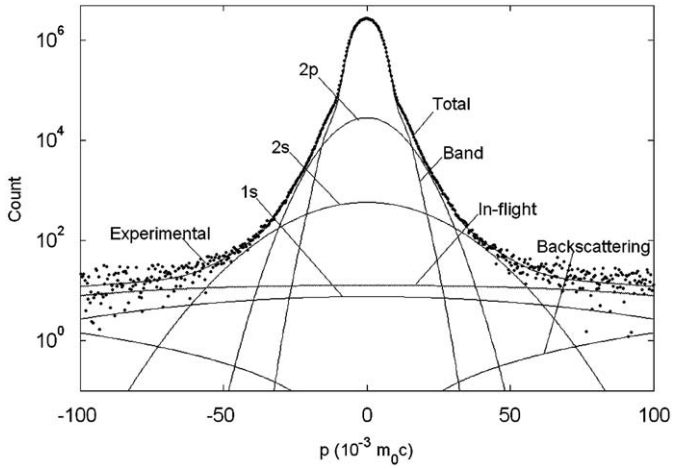

Fig. 3. Fit and experimental Doppler broadening profiles in silicon, including the annihilation with 1s, 2s, 2p, valence band electrons, in-flight positron annihilation, and backscattering.

Table 1
Selection of fitting parameters: relative intensities of positron annihilation with 2p, 2s, 1s, valence band electrons, and in-flight annihilation.

Valence band annihilation	97.44(9)%
2p annihilation	2.45(5)%
2s annihilation	0.103(4)%
1s annihilation	0.0046(2)%
In-flight annihilation[a]	0.066(2)%

[a] In the fit region, these counts were not used in the calculation of percentages of the peak.

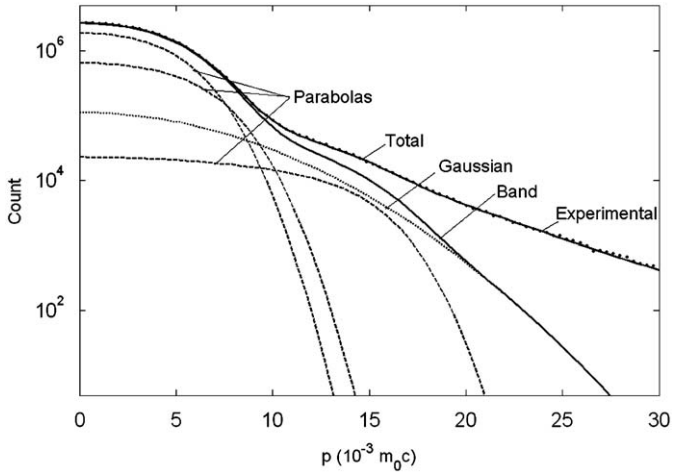

Fig. 4. Fit and experimental Doppler broadening profiles in silicon—details of the valence band, with the three inverted parabolas and the Gaussian.

Table 2
Details of the valence band: annihilation intensities with the parabolas, with the Gaussian, and the parabola cutoff parameters.

Parabola 1	63.0(11)%
Parabola 2	26.4(11)%
Parabola 3	1.82(6)%
Gaussian	6.16(20)%
Cutoff 1	$6.684(14)\times10^{-3}m_oc$
Cutoff 2	$8.28(4)\times10^{-3}m_oc$
Cutoff 3	$16.76(8)\times10^{-3}m_oc$

where n_{ij} is the number of observed events in channel (i,j) of the Doppler broadening real coincidence spectrum, a_{ij} the number of observed events in channel (i,j) of the Doppler broadening accidental coincidence spectrum, and F_{ij} the fitting function. The obtained value was 2.74×10^5 for about 2.50×10^5 degrees of freedom, corresponding to a χ^2 probability of 2×10^{-3}%.

Table 1 shows the intensities of positron annihilation with 2p, 2s, 1s, valence band electrons, and in-flight positron annihilation. The obtained results for the core and valence band electron annihilation intensities were 2.56(9)% and 97.44(9)%, respectively, in agreement with the values reported in the literature [19] of ~2% and ~98%.

In our previous work [29], when 2s shell annihilation intensity in aluminum was fitted with only one Gaussian function, the obtained result was smaller than the theoretical results [7,30,31] and also when compared with the result obtained using two Gaussian functions [9–11]. We also noticed that the 2p intensity had increased to compensate the 2s intensity decrease, whereas the conduction band and 1s shell suffered only minor changes. Therefore, for silicon, where we used a single Gaussian, we expect a similar decrease of the 2s annihilation intensity accompanied by an increase of 2p and no change in the annihilation intensities for the core and the valence band electrons.

Fig. 3 shows the fit and experimental data for projected Doppler broadening profiles, including the 1s, 2s, 2p, valence band electron annihilations, in-flight positron annihilation components, and backscattering. We obtained these profiles by considering a diagonal cross-section of the 2D spectrum with a width of $2m_0c^2-6.18\,\text{keV}<E_1+E_2<2m_0c^2+6.18\,\text{keV}$ projected in the direction E_1-E_2 and resulting in distributions of longitudinal momenta multiplied by c (p_zc), as discussed in Section 2.1. The statistical analysis procedure enables the separation of in-flight positron annihilation and backscattering from other annihilation events in the higher momentum region. It also allows the subtraction of contributions of the ridges, background, and exponential tails that are related to several kinds of scattering and pileup, obtaining a Doppler broadening profile without these contributions.

Fig. 4 is similar to Fig. 3, but shows the fit parabolas and Gaussian that model the photon spectrum from positron annihilation with valence band electrons. Table 2 shows the values obtained for the components of the valence band, namely the intensities of the three parabolas, and one Gaussian and the three parabola cutoff parameters. While parabolas are usually related to conduction band descriptions, here parabolic functions were used because they fit the spectrum better than Gaussian

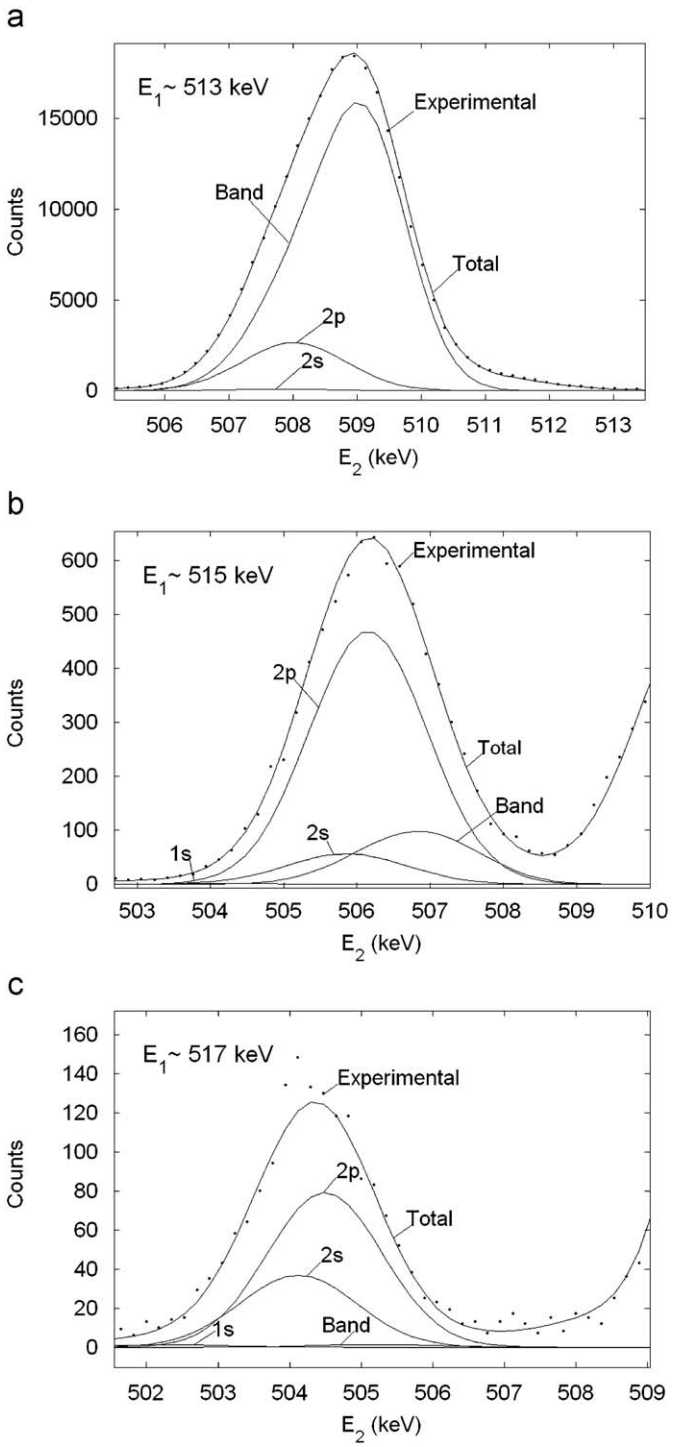

Fig. 5. Measured and fit cross-section of the annihilation component distributions, with the fixed energies in detector 1 of: (a) E_1—513 keV, (b) E_1—515 keV, and (c) E_1—517 keV.

functions. While we quote the results taking into account the energy gap in the Gaussian component and not in the parabolas, the results are not sensitive to the inclusion or exclusion of the gap parameter in the Gaussian and the parabolas, with the other parameters and χ^2 value changing less than their standard deviations in all possible combinations.

Fig. 5 shows sections of the annihilation peak parallel to the energy axis of detector 2 for fixed energies in detector 1, where the experimental data and the corresponding fit function are shown along with 2s, 2p, band, and 1s components. We observe in (a), where the energy in the detector 1 was fixed at about 513 keV, a predominant contribution of the valence band and a small contribution of the annihilation with electrons of the 2p shell with good agreement between the spectrum in detector 2 and the fitting function. In (b), where the energy in the detector 1 was fixed at approximately 515 keV, annihilations with 2p electrons dominate and the fitting function agrees well with the spectrum in detector 2. In (c), with the energy in the detector 1 fixed at approximately 517 keV, contributions of the annihilation with electrons of the 2s shell are important. It is interesting to visualize that the annihilation peak goes to lower energies, moving off the region 511–511 keV due to the decrease in annihilation with lesser bound electrons and a simultaneous increase of annihilation contribution with more strongly bound electrons (with a larger deficit in energy).

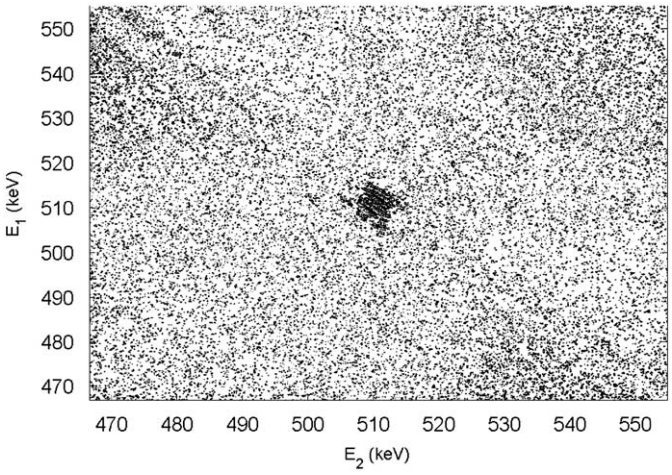

Fig. 6. Contour plot of the relative residue spectrum.

The squares of the relative residues given by

$$\Delta_{ij} = \frac{(n_{ij} - F_{ij})^2}{F_{ij} + 2a_{ij}} \tag{8}$$

are shown in Fig. 6, where two features stand out against the statistical fluctuation. The first is related to the in-flight positron annihilation, where our model was not detailed enough to describe these events in an adequate form. The second is related to the shape of the annihilation peak, where it is possible to note that there were oscillations in residues that are characteristic of a peak with high counting statistics.

We have found that, in this case, a complete DBCS analysis of the electron–positron annihilation radiation is possible. Unlike the usual approach, this procedure allows for the determination of data uncertainties and covariances. Thus, different hypotheses can be tested and results can be obtained from one spectrum.

4. Conclusion

In previous works we applied our DBCS analysis method, consisting of statistical treatment of the experimental spectrum measured in aluminum samples, where we had some success obtaining the annihilation rates, the Fermi momenta, and electron binding energies. Here, we performed measurements in silicon, a semiconductor whose electronic configuration is "similar" to that of aluminum, thus requiring modifications only in the description of the core electrons. Hence, in this work we have extended the applicability of our DBCS analysis method using the statistical treatment of the experimental spectrum, which includes electron binding energies, the Doppler broadening of the annihilation

radiation, in-flight positron annihilation, and energy conservation in the annihilation process, expressed in Eqs. (1) and (2). We also considered the effects of photon interactions with matter such as Compton scattering, backscattering, and pileup for the constitution of the response function of the acquisition system with two HPGe detectors in coincidence. The statistical treatment was based on the non-linear least-squares method to obtain parameters of our model, variances, and covariances in the fit.

Regarding the results of our fit for silicon, they fulfilled our expectations on the shape of annihilation components and response function for the acquisition system and are similar to those in the previous work, where we used aluminum. These results also satisfy basic considerations about positrons interacting with atoms. As can be seen in Fig. 3, the intensity of the 2s (1s) component is smaller than that of the 2p (2p and 2s) component(s), demonstrating that the positrons interact less with electrons nearer to the nuclei (electrons more strongly bound). We can also observe in Fig. 3 that the 2s (1s) component is broader than the 2p (2p and 2s) component(s), demonstrating that the positrons probe electrons with higher momenta for electrons nearer to the nuclei.

We did not find in the literature detailed theoretical calculations of the Doppler broadening profile for silicon as we found for aluminum [7,30,31]. The intensities obtained from the literature [19] for core and valence band annihilation are very close to our experimental values, 2.56(9)% for the core and 97.44(9)% for the valence band, indicating that the model adopted in this work was satisfactory. Thus, the results shown in Tables 1 and 2 are relative intensities of positron annihilation with 2p, 2s, 1s, valence band electrons, and in-flight annihilation and Figs. 3–5 demonstrated that the Doppler broadening profiles obtained directly from the experimental spectrum can be an interesting contribution for new studies.

Although the reduced χ^2 value obtained, 1.096, is very close to unity, showing good overall agreement, it is still not acceptable statistically when considering the number of degrees of freedom, 249 956, reflecting that there are deficiencies in our model: we did not consider annihilations in the ^{22}Na source, positronium formation, and possible sample impurities, among other phenomena that can contribute to this χ^2 value. In addition, this value may be due to the description of longitudinal momentum distributions done following our simple model, where we used only a sum of Gaussians and parabolas, and did not consider more detailed physical calculations. Therefore, our model can be improved to lower χ^2, but its value does not invalidate our results. The fitting DBCS method using simple statistical approaches and the energy conservation principle is a good way to obtain information on the electronic environment where electron–positron annihilation occurs.

Acknowledgements

This work was supported by the Brazilian agencies FAPESP, CNPq, and CAPES. We thank Dr. M.C.A. Fantini for her help with the determination of crystal orientation and Dr. L.M.R. Scolfaro, Dr. M.L.F. Nascimento, and Dr. J.M. Fernández-Varea for discussions.

References

[1] R. Krause-Rehberg, H.S. Leipner, Positron Annihilation in Semiconductors—Defect Studies, Springer Series in Solid-State Sciences, no. 127, Springer, Berlin, Heidelberg, 1999.
[2] M.J. Puska, R.M. Nieminen, Rev. Mod. Phys. 66 (1994) 841.
[3] K.G. Lynn, J.R. MacDonald, R.A. Boie, L.C. Feldman, J.D. Gabbe, M.F. Robbins, E. Bonderup, J. Golovchenko, Phys. Rev. Lett. 38 (1977) 241.
[4] A. Hedgran, D.A. Lind, Phys. Rev. 82 (1951) 126.
[5] K. Shizuma, Nucl. Instr. and Meth. 150 (1978) 447.
[6] Y. Yoshizawa, S. Nakanoda, Y. Kawabata, E. Tanaka, H. Inoue, K. Shizuma, J. Phys. Soc. Japan 53 (1984) 4125.
[7] P.E. Mijnarends, A.C. Kruseman, A. van Veen, H. Schut, A. Bansil, J. Phys.: Condens. Matter 10 (1998) 10383.
[8] P.A. Stern, P. Asoka-Kumar, R.H. Howell, Appl. Surf. Sci. 194 (2002) 71.
[9] E. do Nascimento, Ph. D. Thesis, Institute of Physics, University of São Paulo-IFUSP, Brazil, 2004.
[10] E. do Nascimento, O. Helene, V.R. Vanin, C. Takiya, Braz. J. Phys. 34 (2004) 1017.
[11] E. do Nascimento, O. Helene, V.R. Vanin, C. Takiya, Nucl. Instr. and Meth. A 538 (2005) 723.
[12] S. Dannefaer, W. Puff, D. Kerr, Phys. Rev. B 55 (1997) 2182.
[13] J. Nissilä, K. Saarinen, P. Hautojärvi, Phys. Rev. B 63 (2001) 165202.
[14] M. Alatalo, B. Barbiellini, M. Hakala, H. Kauppinen, T. Korhonen, M.J. Puska, K. Saarinen, P. Hautojärvi, R.M. Nieminen, Phys. Rev. B 54 (1996) 2397.
[15] M. Fujinami, T. Sawada, T. Akahane, Radiat. Phys. Chem. 68 (2003) 631.
[16] M. Hasegawa, Z. Tang, Y. Nagai, T. Nonaka, K. Nakamura, Appl. Surf. Sci. 194 (2002) 76.
[17] M. Fujinami, T. Miyagoe, T. Sawada, T. Akahane, J. Appl. Phys. 94 (2003) 4382.
[18] R.S. Brusa, W. Deng, G.P. Karwasz, A. Zecca, Nucl. Instr. and Meth. B 194 (2002) 519.
[19] M. Hakala, M.J. Puska, R.M. Nieminen, Phys. Rev. B 57 (1998) 7621.
[20] A.W. Hunt, M.H. Weber, J.A. Golovchenko, K.G. Lynn, Appl. Surf. Sci. 149 (1999) 282.
[21] A.W. Hunt, D.B. Cassidy, P.A. Sterne, T.E. Cowan, R.H. Howell, K.G. Lynn, J.A. Golovchenko, Phys. Rev. Lett. 86 (2001) 5612.
[22] M.H. Weber, A.W. Hunt, J.A. Golovchenko, K.G. Lynn, Phys. Rev. Lett. 83 (1999) 4658.
[23] A.W. Hunt, D.B. Cassidy, F.A. Selim, R. Haakenaasen, T.E. Cowan, R.H. Howell, K.G. Lynn, J.A. Golovchenko, Nucl. Instr. and Meth. B 164 (2000) 44.
[24] A.W. Hunt, D.B. Cassidy, F.A. Selim, R. Haakenaasen, T.E. Cowan, R.H. Howell, K.G. Lynn, J.A. Golovchenko, Nature 402 (1999) 157.
[25] N.W. Ashcroft, N.D. Mermin, Solid State Physics, Saunders College Publishing, USA, 1976.
[26] R.B. Firestone, V.S. Shirley, Table of Isotopes, eighth ed., vol. II, Wiley, New York, 1996.
[27] D.W. Marquardt, J. Soc. Appl. Math. 11 (1963) 431.
[28] V.R. Vanin, G. Kenchian, M. Moralles, O. Helene, P.R. Pascholati, Nucl. Instr. and Meth. A 391 (1997) 338.
[29] E. do Nascimento, O. Helene, V.R. Vanin, M.T.F. da Cruz, Nucl. Instr. and Meth. B 247 (2006) 38.
[30] Z. Tang, M. Hasegawa, Y. Nagai, M. Saito, Y. Kawazoe, Phys. Rev. B 65 (2002) 045108.
[31] V.J. Gosh, M. Alatalo, P. Asoka-Kumar, B. Nielsen, K.G. Lynn, A.C. Kruseman, P.E. Mijnarends, Phys. Rev. B 61 (2000) 10092.